OPEN ACCESS
Journal of Innovative Optical Health Sciences
Vol. 14, No. 4 (2021) 2141007 (10 pages)

DOI: 10.1142/S1793545821410078

World Scientific
www.worldscientific.com

Synthesis and characterization of reporter molecules embedded core-shell nanoparticles as SERS nanotags

Chloe Duffield, Nana Lyu and Yuling Wang*
Department of Molecular Sciences
ARC Centre of Excellence for Nanoscale BioPhotonics
Faculty of Science and Engineering, Macquarie University
Sydney, NSW 2109, Australia
**yuling.wang@mq.edu.au*

Received 27 April 2021
Accepted 31 May 2021
Published 27 July 2021

Surface-enhanced Raman scattering (SERS) spectroscopy is presented as a sensitive and specific molecular tool for clinical diagnosis and prognosis monitoring of various diseases including cancer. In order for clinical application of SERS technique, an ideal method of bulk synthesis of SERS nanoparticles is necessary to obtain sensitive, stable and highly reproducible Raman signals. In this contribution, we determined the ideal conditions for bulk synthesis of Raman reporter (Ra) molecules embedded silver-gold core-shell nanoparticles (Au@Ra@ AgNPs) using hydroquinone as reducing agent of silver nitrate. By using UV-Vis spectroscopy, Raman spectroscopy and transmission electron microscopy (TEM), we found that a 2:1 ratio of silver nitrate to hydroquinone is ideal for a uniform silver coating with a strong and stable Raman signal. Through stability testing of the optimized Au@Ra@AgNPs over a two-week period, these SERS nanotags were found to be stable with minimal signal change occurred. The stability of antibody linked SERS nanotags is also crucial for cancer and disease diagnosis, thus, we further conjugated the as-prepared SERS nanotags with anti-EpCAM antibody, in which the stability of bioconjugated SERS nanotags was tested over eight days. Both UV-Vis and SERS spectroscopy showed stable absorption and Raman signals on the anti-EpCAM conjugated SERS nanotags, indicating the great potential of the synthesized SERS nanotags for future applications which require large, reproducible and uniform quantities in order for cancer biomarker diagnosis and monitoring.

Keywords: Surface-enhanced Raman spectroscopy; gold nanoparticles; Raman reporter molecules; SERS nanotags and bioconjugation.

*Corresponding author.

1. Introduction

In a climate of major socio-economic burden as a consequence of diseases, the demand for cost effective, rapid and accurate detection is ever increasing for clinical diagnosis purposes. The use of plasmonic nanoparticles as tags or probes presents an accurate, highly sensitive and molecule specific method using surface-enhanced Raman scattering (SERS) spectroscopy to detect low-concentrations of biomarkers for disease quantification and identification.[1–4] The potential of these particles is applicable to many applications and innovative technologies for medical diagnosis such as the use of lateral flow assays for cytokine and disease detection due to the ability for extremely low concentrations of biomarkers to be detected through SERS enhancement.[5,6] However, in order for nanoparticle used in further technologies and applications, it is vital that their synthesis being optimized and controlled for bulk synthesis.

In previous studies conducted, different plasmonic structures have been synthesized including stars, spheres, shells and rods.[7–13] For example, gold/silver nanostars have been demonstrated to induce very high SERS signal due to the spikes present on the surface which act as SERS "hot spots".[14–18] However, their structure is difficult to ensure reproducibility due to the unpredictability of the shape and size of the spikes in their structure.[19–23] The spherical design of the nanoparticles is easier to control and ensure uniformity due to the nature of the synthesis process required. While the signal is less than the nanostars at the fundamental level, this could be improved through the addition of another plasmonic layer, e.g., silver coating in the nanoparticle synthesis which amplifies the plasmonic resonance and consequential Raman signal.[10,20,24–26] With concerns have been expressed about the requirement for aggregation, with the added silver coating, and optimization of the synthesis conditions to increase the thickness of the outer silver layer, an increased SERS response could be obtained. The subsequent testing conducted in our studies aimed at identifying the ideal synthesis conditions in order to meet this need of reproducibility and stability whilst ensuring the highest possible SERS signal using spherical nanoparticles.

In a previous study conducted by Zhang *et al.* on the synthesis of silver coated spherical nanoparticles, their study showed an increased Raman signal through the addition of 60 μL for both hydroquinone and silver nitrate on gold nanoparticles.[26] It is thus assumed that varying the ratios between hydroquinone and silver nitrate would have an effect on the synthesis and the corresponding Raman signals. Consequently, the method proposed in the previous study found that while doubling the amount of both hydroquinone and silver nitrate, the Raman signal increased compared to that without coating. Therefore, it is very important to investigate on which reacting component caused the enhanced effect and whether the amounts (or ratio) of different reactants could be optimized for bulk synthesis. Thus, for our methodology we aimed at varying the ratios in order to test these conditions. Another critical factor in order to ensure the further applications being conducted with reliability, the stability of the synthesized silver coated gold and bioconjugated spherical nanoparticles was also monitored for changes in their UV-Vis absorption intensity and SERS signal. In doing so, the stability of the as-prepared SERS nanotags ensures their reliability, uniformity and accuracy in quantitative uses after being transported and stored for an amount of time.

SERS nanotags have been reported in various applications including cytokine, DNA mutation, cancer and virus detection through the attachment of ligand molecules, such as antibodies to the SERS nanotags.[27–29] The specific antibodies then attach to corresponding biomarkers for quantitative detection purposes using SERS. Through the use of specific ligand molecule (e.g., antibodies), biomarkers are able to be detected and quantified for the characterization and identification of diseases in a rapid manner.[1,5,9,19,27] For instance, the use of SERS nanotags has been demonstrated to detect specific mutations within the EpCAM gene which are often associated with Lynch syndrome that increases the chance of various cancers such as colon and breast cancer.[27–29] Among this, the stability of the antibody-conjugated nanotags is crucial to ensure the bonding of the corresponding biomarkers and thus, impacts the accuracy of the consequential signal from SERS.[30,31] In our previous study, we have tested the antibody conjugated SERS nanotags in one buffer type.[10] Following on our previous studies, to demonstrate the potential application of the as-prepared SERS nanotags in biomedical diagnosis, it is vital to determine the most ideal storage conditions that ensures product stability for future biomedical application. We thus further

demonstrated the bioconjugation of anti-EpCAM antibody on the as-prepared SERS nanotags, and test their stability in four different buffers. By using UV-Vis absorption and SERS spectroscopy, we have demonstrated the stability of anti-EpCAM conjugated SERS nanotags in 0.05%BSA/PBS, and 0.05%BSA/HEPES buffer over 8 days. Therefore, in this study, we aimed at optimizing the synthesis conditions for both silver coated gold nanoparticles and bioconjugated nanoparticles with antibodies, and determining their stability for the bulk synthesis of the designed nanotags for potential future applications in biomedical diagnosis.

2. Materials and Methods

2.1. *Materials and reagents*

All reagents including gold(III) chloride trihydrate ($HAuCl_4 \cdot 3H_2O$), sodium citrate tribasic dihydrate, silver nitrate, hydroquinone, 4-(2-hydroxyethyl)-1-piperazine ethane sulfonic acid (HEPES) bovine serum albumin (BSA), 5,5-dithio-bis-(2-nitrobenzoic acid) (DTNB) and 3,3′-dithiobis(sulfosuccinimidyl propionate) (DTSSP) were purchased from Sigma-Aldrich (Sydney, Australia), unless otherwise stated. Anti-EpCAM (monoclonal mouse IgG_{2B} Clone, MAB9601) were obtained from R&D systems (In Vitro Technologies, Australia). Milli-Q water (18.2 MΩ.cm) was used to prepare all aqueous solutions.

2.2. *Methods*

2.2.1. *Synthesis of DTNB-coated AuNPs (Au@DTNB)*

Gold nanoparticles (AuNPs) at size of approximately 60 nm were synthesized by heating $HAuCl_4$ aqueous solution (0.01% w/v, 50 mL) to boiling under stirring at 600 rpm, following with addition of 0.35 mL sodium citrate solution (1.0% w/v), the color of the solution changed from faint blue to bright purple within 2 min after addition of the sodium citrate. The solution was boiled and stirred continuously for another 20 min before cooling down to room temperature. To obtain SERS nanotags, 10 μL of 1 mM of DTNB dissolved in ethanol was added to 1 mL as-prepared AuNPs under shaking for 12 h to ensure a complete DTNB-coated AuNPs (Au@DTNB) surface. Excess DTNB molecules were removed by centrifugation at 5000 rpm for 7 min and the pellet was then re-dispersed in water for the following use.

2.2.2. *Synthesis of silver coated Au@DTNB*

The silver coating on Au@DTNB was performed by adding 30 μL of hydroquinone (10 mM) and different volumes (15, 30, 45, 60, 75, and 90 μL) of $AgNO_3$(10 mM), sequentially. The solution was then incubated overnight to ensure the formation of a silver coating on the Au@DTNB. The as-prepared Au@DTNB@AgNPs were then centrifuged at 6000 rpm for 6 min to remove excess $AgNO_3$ and hydroquinone, then re-suspended in Milli-Q water.

2.2.3. *Bioconjugation of anti-EpCAM antibody on Au@DTNB@AgNPs*

For preparation of the monoclonal antibody conjugated SERS nanotags, DTSSP (8 μL, 1 mg/mL) was mixed with anti-EpCAM antibody (8 μL, 0.5 μg/μL in PBS) and incubated under 300 rpm shaking at room temperature for 30 min. 16 μL of DTSSP-EpCAM antibody was then added to 0.5 mL Au@DTNB@AgNPs and incubated at room temperature for another 30 min. The sample was then left at 4°C overnight to ensure conjugation of antibodies to the surface of Au@DTNB@AgNPs. To remove excess DTSSP linker and antibodies, the SERS nanotags were centrifuged at 4°C for 10 min at 6000 rpm. For further testing, the antibody-conjugated SERS nanotags were re-dispersed in 300 μL of different buffer solution including 0.05% BSA in 0.1 mM PBS, 0.05% BSA in HEPES, 0.1 mM PBS or 0.1 mM HEPES.

2.3. *Instrument*

SERS spectra of the as-prepared Au@DTNB@AgNPs were collected using portable Raman microscope (IM-52, Snowy Range Instruments) at 785 nm excitation with the 70 mW laser power, 1 s of integration time for six accumulations. Transmission electron microscope (TEM, Philips CM10) was used to observe the size and morphology of the particles. The size distribution and zeta potential of the AuNPs and Au@DTNB@AgNPs were determined using Zetasizer NanoZS (Malvern U.K.). The plasmonic resonance of AuNPs and

Au@DTNB@AgNPs was detected using UV-Vis spectrometer (NanoDrop 2000, Thermo Scientific).

3. Results and Discussion

3.1. *Synthesis of silver coated Ra embedded gold nanoparticles*

The silver-coated Ra-Au nanoparticles (Au@Ra@AgNPs) were designed using a gold core coated with Raman reporter molecules (Ra). Initially, DTNB were used as the Raman reporter molecule which binds to the gold core through an Au–S bond, forming a self-assembled monolayer (SAM) as indicated in Scheme 1. DTNB is able to form the SAM on gold through the breakage of the disulfide bond.[32,33] The silver layer was generated via the hydroquinone reduction of $AgNO_3$.[10] The advantages of this design include (i) the further amplified SERS signal due to the plasmonic coupling effect of gold–silver upon silver coating, and (ii) the protection of Raman reporter molecules to ensure a stable Raman signal owing to the embedded molecule in the core-shell structure.

During the synthesis, we observed a color change from pink/purple by the AuNPs to an orange/brown as a consequence of the increasing silver nitrate volumes indicating the formation of the silver layer onto the Au@DTNB. As displayed in Fig. 1, whereby with an increasing ratio between silver nitrate and hydroquinone, the color becomes more orange. Beyond a 2:1 ratio of silver nitrate to hydroquinone, the samples became more aggregated and less silver coating was observed. A study of the varying ratios of hydroquinone was also tested and was found to have minimal to no impact on the overall reaction.

3.2. *Characterization of silver coated Ra embedded gold nanoparticles*

For the characterization of the AuNPs and SERS nanotags, we performed UV-Vis absorption spectroscopy for the surface plasmonic resonance (SPR) of each sample. As seen in Fig. 2, the characteristic SPR peak shifted with the varying volumes of silver nitrate compared to the AuNPs and Au@DTNB. The peak of AuNPs is situated at roughly 540 nm while the peak for Au@DTNB is shifted at 550 nm due to the binding of DTNB on AuNPs surface, which is induced by the change of the surrounding refractive index when DTNB forms SAM on AuNPs.[34] Compared to the control experiment (30 μL of silver nitrate without hydroquinone), when the hydroquinone was added, the blue shift of the SPR peak occurred, indicating the silver layer has formed. The peak shift varies with the different volumes of $AgNO_3$ which is a consequence of the different thickness of the silver layer. As seen in the 2:1 ratio of silver nitrate (60 μL) to hydroquinone, whereby the peak shifts to 525 nm, indicating the thickest silver coating based on the corresponding peak. With the silver nitrate to hydroquinone ratio increasing (2.5:1 and 3:1), much broader SPR bands (green and blue curves in Fig. 2) were observed,

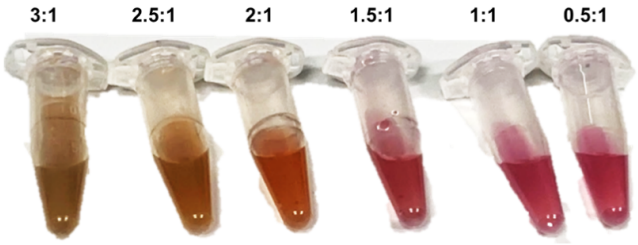

Fig. 1. Photograph of as-prepared Au@DTNB@AgNPs at different ratios of silver nitrate to hydroquinone.

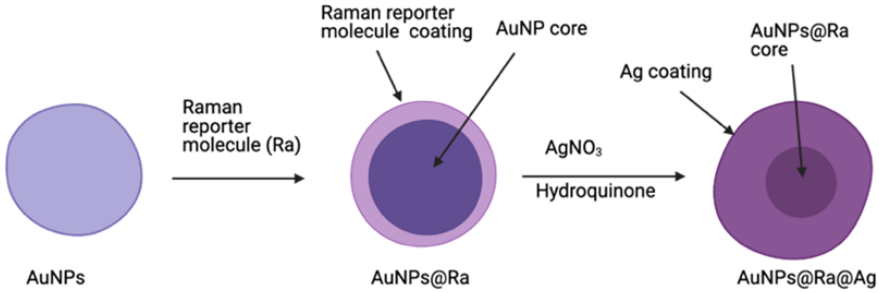

Scheme 1. The scheme for synthesis of silver-coated AuNPs-Ra SERS nanotags.

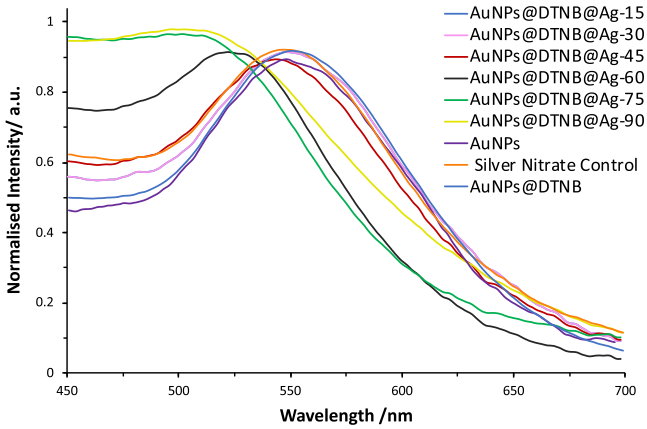

Fig. 2. UV-Vis absorption spectra of AuNPs, Au@DTNB and Au@DTNB@AgNPs with varying silver nitrate volumes and the control without hydroquinone.

which is an indication of the aggregation induced by high amount of silver nitrate.

We further measured the size of AuNPs, Au@DTNB and Au@DTNB@AgNPs using TEM images (Fig. 3), which show the silver coating as indicated by the lighter region around the darker gold sphere core. As the ratio of silver nitrate to hydroquinone increased, the Au@DTNB@AgNPs tend to aggregate, and less silver coating is applied. Hence, the lighter region of silver around the particles is minimal as compared to 2:1 ratio of silver nitrate (60 μL) to hydroquinone. The thickness of silver layer for the ideal ratio of 2:1 of silver nitrate to hydroquinone was found to be 5–7 nm. As the small Raman reporter molecule (DTNB) was embedded between the gold core and silver layer, it is assumed the gap between gold and silver is less than 1 nm. However, this gap is too small to be seen within the TEM images due to the low resolution of the TEM microscope used in this study.

Thus, the silver coating of AuNPs@DTNB has been confirmed through both UV-Vis spectroscopy (Fig. 2) and TEM imaging (Fig. 3). The UV-Vis spectroscopy shows the blue shift of the as-prepared nanoparticles as a consequence of the change in surface plasmon resonance with the formation of silver layer, whereby its dielectric constant causes the blue shift and confirms the silver coating. The TEM images show an inner darker, denser region of gold core and a lighter outer region of silver layer, which further confirms the formation of the silver layer on gold core.

To better understand the physical mechanism behind SERS enhancement after the silver coating and establish the relationship of the as-prepared nanoparticles with their Raman signal, the UV-Vis characterizations and TEM images were compared with the corresponding Raman intensities. As seen in Fig. 4, the characteristic Raman vibrational peaks of DTNB are located at 1334 and 1560 cm^{-1}, which is a consequence of the asymmetric NO_2 stretching and aromatic ring vibration, respectively.[2,35] When the volume of silver nitrate increased for the synthesis, the Raman signal increased which indicated the formation of the silver layer which generates stronger surface plasmonic resonance effects to amplify the Raman scattering of DTNB. However, the Raman signal increased dramatically when the volume of silver nitrate increased to 75 μL or 90 μL, which may be due to the increase of silver thickness or the formation of aggregate during synthesis. The formation of aggregates will

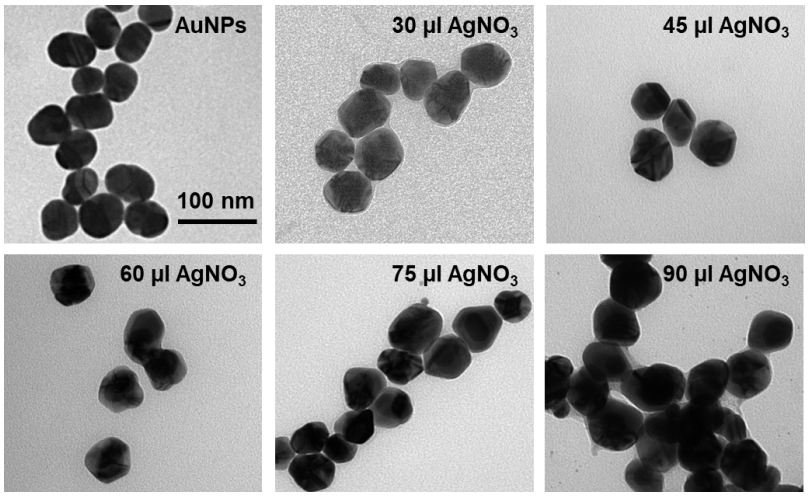

Fig. 3. TEM images of Au@DTNB@AgNPs at varying volume of silver nitrate.

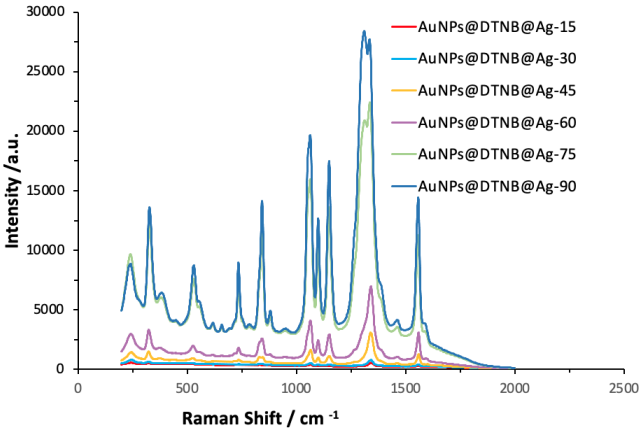

Fig. 4. SERS spectra of DTNB for varying silver nitrate volumes and controls.

introduce significant signal variations which result in imprecise and inaccurate signals for quantitative analysis. The most uniform and thickest coating was thus achieved through a 2:1 ratio of silver nitrate to hydroquinone, which also resulted in the highest SERS enhancement and aligned with the results from the UV-Vis and SERS spectroscopy. Moreover, due to the small size of the Raman reporter molecules (DNTB) embedded between gold core and silver shell, this small interior gap (~ 1 nm) is assumed to generate a SERS enhancement factor about 6.0×10^5–5.0×10^6 as reported,[10,36–38] though the DNA-based gap-enhanced Raman scattering would produce about 1.0×10^8 –2.0×10^9 enhancement.[39,40] The extremely high SERS enhancement factor is attributed to the strong electromagnetic field associated with the localized surface plasmon coupling effect due to the interior gap.[40–43]

We further investigated the characteristics of the Au@DTNB@AgNPs through the determination of zeta potential (Table 1) in order to gauge their isoelectric stability. As compared to AuNPs and Au@DTNB, the zeta potential tended to become increasingly negative to a peak at 1.5:1 ratio. The values decreased from -30.5 ± 0.7, -30.2 ± 11.3, -29.5 ± 0.8, -31.6 ± 0.7, -33.4 ± 1.5, -31.6 ± 0.6, -28.8 ± 3.1, and -30.6 ± 1.5 mV for AuNPs, Au@DTNB and each increasing ratio of silver nitrate to hydroquinone, sequentially. As indicated in Table 1, beyond the 1.5:1 ratio of silver nitrate to hydroquinone, the values increase slightly. This indicates that as increasing amounts of silver nitrate are added, the Au@DTNB@AgNPs become more stable until the 1.5:1 ratio; beyond which the particles become less stable and are more prone to aggregation. This can also be seen in the TEM images within Fig. 4 whereby the samples tend to become more aggregated within the 2.5:1 ratio and beyond.

Table 1. Zeta potential of as-prepared nanoparticles.

Sample	Zeta potential (mV)
AuNPs (60 nm)	-30.5 ± 0.7
AuNPs@DTNB	-30.2 ± 1.3
AuNPs@DTNB@Ag15	-29.5 ± 0.8
AuNPs@DTNB@Ag30	-31.6 ± 0.7
AuNPs@DTNB@Ag45	-33.4 ± 1.5
AuNPs@DTNB@Ag60	-31.6 ± 0.6
AuNPs@DTNB@Ag75	-28.8 ± 3.1
AuNPs@DTNB@Ag90	-30.6 ± 1.5
Hydroquinone control 0:1	-30.4 ± 2.7
$AgNO_3$ control 1:0	-26.0 ± 0.5

According to the results from UV-Vis, SERS, TEM and Zeta-potential of as-prepared nanoparticles, it was determined that the ideal ratio of 2:1 between silver nitrate and hydroquinone for the bulk synthesis of Au@DTNB@AgNPs is the most stable condition from aggregates and has the thickest silver coating which increases SERS intensity due to surface plasmonic effects.

3.3. *Stability study of silver coated Ra embed gold nanoparticles*

Moreover, the stability of AuNPs@DTNB@Ag in a 2:1 ratio was tested using UV-Vis spectroscopy and Raman spectroscopy over two weeks to ensure their potential for further medical applications. As shown in Table 2, the stability study did not show any significant changes to the SERS intensity nor were any significant aggregates formed. Both of Raman intensity and UV-Vis absorption intensity remained fairly consistent over the week that the sample was measured, thus concluding that the samples are able to be kept for further medical applications without significant changes or aggregation. Although the readings to show variation, this is consistent with the Raman and UV-Vis readings which can be quite sensitive to minor changes.

3.4. *Bioconjugation of antibodies onto silver coated Ra embed gold nanoparticles*

Due to the transportation and storage of potential future products, the products ability to produce

Table 2. Stability study of Au@DTNB@AgNPs using UV-Vis and Raman spectroscopy.

Day	UV-Vis intensity (a.u.)	Wavelength (nm)	Raman shift (cm^{-1})	Raman intensity (a.u.)
Day 1	0.110	536	1345.31	817.22
Day 3	0.126	534	1343.02	864.98
Day 8	0.122	535	1344.94	819.09

accurate and precise measurements over time relies on its stability. For further clinical application, a stability study was conducted on the biconjugated silver coated gold nanoparticles in order to test their longevity. Scheme 2 illustrates the process of bioconjugation whereby, the DTSSP linker is added to the Au@DTNB@AgNPs before adding the EpCAM antibodies which were covalently bounded to the surface of nanoparticles. DTSSP was used as the linker because it has an ester group to react with the primary amino group in antibody for direct bioconjugation (as shown in Scheme 2). Compared to the linker of 11-mercaptoundecanoic acid (MUA), which requires an additional activation step via EDC/NHS (1-ethyl-3-(3-dimethylaminopropyl) carbodiimide hydrochloride/N-Hydroxysuccinimide) coupling chemistry to activate the carboxyl group for antibody conjugation, DTSSP provides an easier reaction whereby it was first mixed with the antibodies to maximize bonding before being added to the Au@DTNB@AgNPs to form the antibody conjugated SERS nanotags.

3.5. *Stability study of EpCAM-silver coated Ra embed gold nanoparticles*

The stability of EpCAM antibody conjugated Au@DTNB@AgNPs was tested in four different buffer solution to determine which buffer is the most suitable condition for product distribution in terms of the aggregation and Raman signal. Table 3 shows the signal intensity from UV-Vis and Raman spectroscopy. The results indicated that the 0.05% BSA in 0.1 mM PBS was the ideal buffer that ensured the greatest stability by comparison of the UV-Vis intensity to the corresponding Raman intensity, which demonstrates high levels of nanoparticles stability over time. The large changes in these values occurred due to aggregation in the sample which can either significantly increase or decrease the signal. Without PBS, the particles tended to have much higher level of aggregation which consequentially resulted in changes in Raman intensity as well as the absorption intensity. While different buffers showed some variability, this is typical due

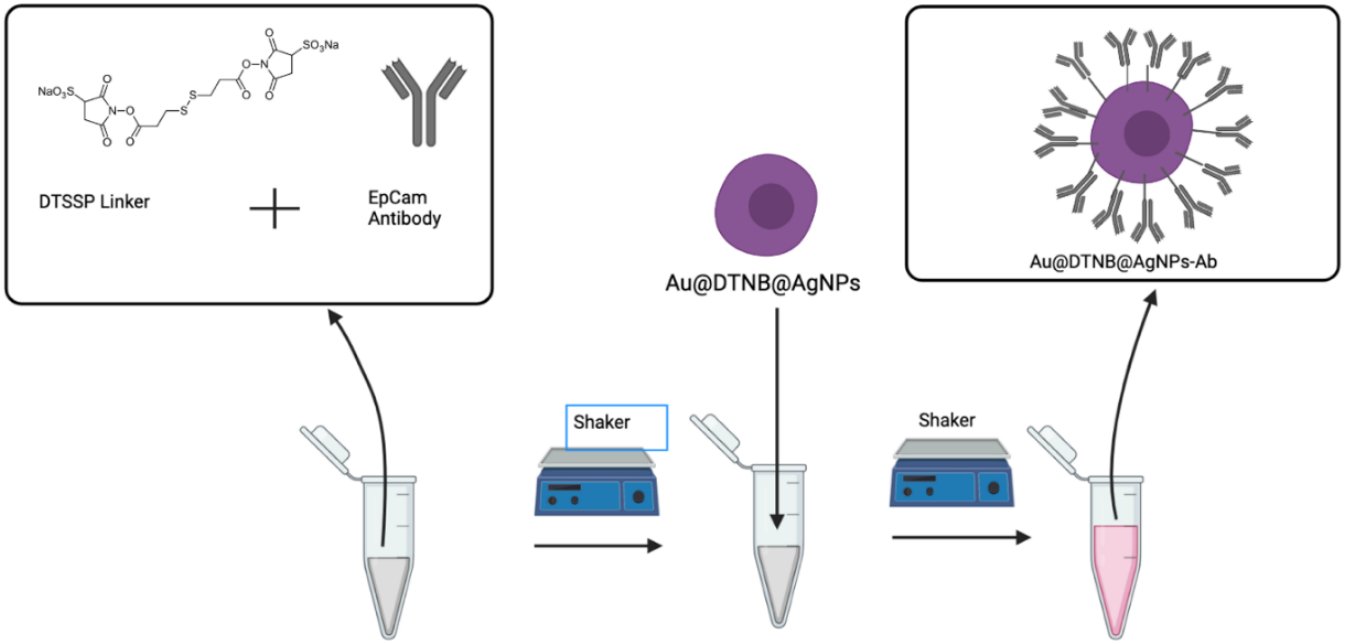

Scheme 2. Bioconjugation of EpCAM antibodies onto the Au@DTNB@AgNPs.

Table 3. Stability study of EpCAM antibody conjugated Au@DTNB@AgNPs in various buffers.

Day	Buffer type	UV-Vis intensity (a.u.)	Wavelength (nm)	Raman shift (cm^{-1})	Raman intensity (a.u.)
Day 1	0.05% BSA in 0.1 mM PBS	0.051	565	1345.75	707.42
	0.05% BSA in 0.1 mM HEPES	0.108	567	1344.22	545.27
	0.1 mM PBS	0.080	573	1341.16	584.27
	0.1 mM HEPES	0.028	588	1342.64	916.73
Day 4	0.05% BSA in 0.1 mM PBS	0.115	559	1344.04	762.65
	0.05% BSA in 0.1 mM HEPES	0.143	552	1342.91	701.89
	0.1 mM PBS	0.117	561	1342.61	770.24
	0.1 mM HEPES	0.095	572	1341.99	1097.46
Day 7	0.05% BSA in 0.1 mM PBS	0.106	557	1343.21	701.81
	0.05% BSA in HEPES 0.1 mM	0.065	569	1342.12	739.39
	0.1 mM PBS	0.079	569	1342.92	527.97
	0.1 mM HEPES	0.081	570	1344.00	687.38

to the aggregating nature of the particles. For further clinical applications, a more stable buffer must be used in order to ensure consistency within the samples used as aggregation can cause major changes to consequent readings. It should also be mentioned that the proposed Raman reporter embedded SERS nanotags were designed for *in vitro* applications whereby the toxicity of silver in biological systems is not an issue. However, a biocompatible layer such as BSA or polyethylene glycol (PEG) can be easily coated on the SERS nanotags surface to improve its potential application for the *in vivo* study.

4. Conclusion

In summary, we have determined the ideal method of synthesis of SERS nanotags consisting of a gold core, Raman reporter molecules and silver layer using hydroquinone as the reducing agent. Due to the surface plasmon coupling resonance effect within the interior gap (so-called gap-enhanced Raman scattering) between the gold core and the silver layer, SERS signal was increased significantly with the increase of silver shell thickness, allowing for high sensitivity and specificity in the future clinical applications. The synthesis of silver nanoparticles was determined to be ideal when in a 2:1 ratio of silver nitrate to hydroquinone. This allowed for the highest SERS signal and thus improving the synthesis of new SERS nanotags for diagnostic purposes. The silver coated AuNPs were found to be stable as per stability testing over two-week period using UV-Vis and Raman spectroscopy. When the SERS nanotags were bioconjugated with an antibody, they were tested against various buffers. SERS nanotags showed the highest stability when they were suspended in PBS containing 0.05% BSA, providing the ideal condition of SERS nanotags which are stable for future medical applications.

Conflicts of Interest

The authors declare that there are no conflicts of interest relevant to this article.

Acknowledgment

This work was supported by the Australian Research Council (ARC) through its Centre of Excellence for Nanoscale BioPhotonics (CE140100003) and ARC Discovery Projects (DP200102004).

References

1. D. Flieger, A. S. Hoff, T. Sauerbruch, I. G. Schmidt-Wolf, "Influence of cytokines, monoclonal antibodies and chemotherapeutic drugs on epithelial cell adhesion molecule (EpCAM) and LewisY antigen expression," *Clin. Exp. Immunol.* **123**(1), 9–14 (2001).
2. J. Li, A. Wuethrich, A. A. I. Sina, H.-H Cheng, Y. Wang, A. Behren, P. N. Mainwaring, M. Trau, "A digital single-molecule nanopillar SERS platform for predicting and monitoring immune toxicities in immunotherapy," *Nat. Commun.* **12**(1), 1087 (2021).
3. S. Tsao, J. Wang, Y. Wang, A. Behren, J. Cebon, M. Trau, "Characterising the phenotypic evolution

of circulating tumour cells during treatment," *Nat. Commun.* **9**, 1482 (2018).
4. W. Zhang, L. Jiang, R. J. Diefenbach, D. H. Campbell, B. J. Walsh, N. H. Packer, Y. Wang, "Enabling sensitive phenotypic profiling of cancer-derived small extracellular vesicles using surface-enhanced Raman spectroscopy nanotags," *ACS Sensors* **5**(3), 764–771 (2020).
5. W. Xie, S. Schlücker, "Medical applications of surface-enhanced Raman scattering," *Phys. Chem. Chem. Phys.* **15**(15), 5329–5344 (2013).
6. N. Lyu, V. K. Rajendran, R. J. Diefenbach, K. Charles, S. J. Clarke, A. Engel, Sydney Colorectal Cancer Study Investigators, H. Rizos, M. P. Molloy, Y. Wang, "Multiplex detection of ctDNA mutations in plasma of colorectal cancer patients by PCR/SERS assay," *Nanotheranostics* **4**(4), 224–232 (2020).
7. J. Jana, M. Ganguly, T. Pal, "Enlightening surface plasmon resonance effect of metal nanoparticles for practical spectroscopic application," *RSC Adv.* **6**(89), 86174–86211 (2016).
8. K. Kamil Reza, J. Wang, R. Vaidyanathan, S. Dey, Y. Wang, M. Trau, "Electrohydrodynamic-induced SERS immunoassay for extensive multiplexed biomarker sensing," *Small* **13**(9), 1602902 (2017).
9. Y. Liu, N. Lyu, V. K. Rajendran, J. Piper, A. Rodger, Y. Wang, "Sensitive and direct DNA mutation detection by surface-enhanced raman spectroscopy using rational designed and tunable plasmonic nanostructures," *Anal. Chem.* **92**(8), 5708–5716 (2020).
10. D. Li, L. Jiang, J. A. Piper, I. S. Maksymov, A. D. Greentree, E. Wang, Y. Wang, "Sensitive and multiplexed SERS nanotags for the detection of cytokines secreted by lymphoma," *ACS Sensors* **4**(9), 2507–2514 (2019).
11. Y. Zhang, P. Yang, M. A. Habeeb Muhammed, S. K. Alsaiari, B. Moosa, A. Almalik, A. Kumar, E. Ringe, N. M. Khashab, "Tunable and linker free nanogaps in core–shell plasmonic nanorods for selective and quantitative detection of circulating tumor cells by SERS," *ACS Appl. Mater. Interf.* **9**(43), 37597–37605 (2017).
12. W. Shen, X. Lin, C. Jiang, C. Li, H. Lin, J. Huang, S. Wang, G. Liu, X. Yan, Q. Zhong, B. Ren, "Reliable quantitative SERS analysis facilitated by core-shell nanoparticles with embedded internal standards," *Angew. Chem. Int. Ed. Engl.* **54**(25), 7308–7312 (2015).
13. Y. Feng, Y. Wang, H. Wang, T. Chen, Y. Y. Tay, L. Yao, Q. Yan, S. Li, H. Chen, "Engineering "hot" nanoparticles for surface-enhanced raman scattering by embedding reporter molecules in metal layers," *Small* **8**(2), 246–251 (2012).
14. J. Reguera, J. Langer, D. Jiménez de Aberasturi, L. M. Liz-Marzán, "Anisotropic metal nanoparticles for surface enhanced Raman scattering," *Chem. Soc. Rev.* **46**(13), 3866–3885 (2017).
15. V. Tran, C. Thiel, J. T. Svejda, M. Jalali, B. Walkenfort, D. Erni, S. Schlücker, "Probing the SERS brightness of individual Au nanoparticles, hollow Au/Ag nanoshells, Au nanostars and Au core/Au satellite particles: Single-particle experiments and computer simulations," *Nanoscale* **10**(46), 21721–21731 (2018).
16. C. L. Zavaleta, B. R. Smith, I. Walton, W. Doering, G. Davis, B. Shojaei, M. J. Natan, S. S. Gambhir, "Multiplexed imaging of surface enhanced Raman scattering nanotags in living mice using noninvasive Raman spectroscopy," *PNAS* **106**(32), 13511–13516 (2009).
17. J.-H. Kim, H. Kang, S. Kim, B.-H. Jun, T. Kang, J. Chae, S. Jeong, J. Kim, D. H. Jeong, Y.-S. Lee, "Encoding peptide sequences with surface-enhanced Raman spectroscopic nanoparticles," *Chem. Commun.* **47**(8), 2306–2308 (2011).
18. Y. Yang, C. Gu, J. Li, "Sub-5 nm metal nanogaps: Physical properties, fabrication methods, and device applications," **15**(5), 1804177 (2019).
19. V. Tran, B. Walkenfort, M. König, M. Salehi, S. Schlücker, "Rapid, quantitative, and ultrasensitive point-of-care testing: A portable SERS reader for lateral flow assays in clinical chemistry," *Angew. Chem. Int. Edn.* **58**(2), 442–446 (2019).
20. A. M. Fales, T. Vo-Dinh, "Silver embedded nanostars for SERS with internal reference (SENSIR)," *J. Mater. Chem. C* **3**(28), 7319–7324 (2015).
21. J. Wang, K. M. Koo, Y. Wang, M. Trau, "Engineering state-of-the-art plasmonic nanomaterials for SERS-based clinical liquid biopsy applications," *Adv. Sci.* **6**(23), 1900730 (2019).
22. K. Mahato, S. Nagpal, M. A. Shah, A. Srivastava, P. K. Maurya, S. Roy, A. Jaiswal, R. Singh, P. Chandra, "Gold nanoparticle surface engineering strategies and their applications in biomedicine and diagnostics," *3 Biotech* **9**(2), 57 (2019).
23. T. Yang, J. Jiang, "Embedding Raman tags between Au nanostar@nanoshell for multiplex immunosensing," *Small (Weinheim an der Bergstrasse, Germany)* **12**(36), 4980–4985 (2016).
24. B. Khlebtsov, N. Khlebtsov, "Surface-enhanced Raman scattering-based lateral-flow immunoassay," *Nanomaterials (Basel)* **10**(11), 2228 (2020).
25. Y. Wang, R. Vaidyanathan, M. J. A. Shiddiky, M. Trau, "Enabling rapid and specific surface-enhanced Raman scattering immunoassay using nanoscaled surface shear forces," *ACS Nano* **9**(6), 6354–6362 (2015).

26. Y. Zhang, L. Lin, J. He, J. Ye, "Optical penetration of surface-enhanced micro-scale spatial offset Raman spectroscopy in turbid gel and biological tissue," *J. Innov. Opt. Health Sci.* 2141001 (2021).
27. L. Huang, Y. Yang, F. Yang, S. Liu, Z. Zhu, Z. Lei, J. Guo, "Functions of EpCAM in physiological processes and diseases (review)," *Int. J. Mol. Med.* **42**(4), 1771–1785 (2018).
28. B. T. van der Gun, L. J. Melchers, M. H. Ruiters, L. F. de Leij, P. M. McLaughlin, M. G. Rots, "EpCAM in carcinogenesis: The good, the bad or the ugly," *Carcinogenesis* **31**(11), 1913–1921 (2010).
29. D. Liu, J. Sun, J. Zhu, H. Zhou, X. Zhang, Y. Zhang, "Expression and clinical significance of colorectal cancer stem cell marker EpCAM(high)/CD44(+) in colorectal cancer," *Oncol. Lett.* **7**(5), 1544–1548 (2014).
30. J. Wang, W. Anderson, J. Li, L. L. Lin, Y. Wang, M. Trau, "A high-resolution study of in situ surface-enhanced Raman scattering nanotag behavior in biological systems," *J. Coll. Interf. Sci.* **537**, 536–546 (2019).
31. V. Tran, B. Walkenfort, M. König, M. Salehi, S. Schlücker, "Rapid, quantitative, and ultrasensitive point-of-care testing: A portable SERS reader for lateral flow assays in clinical chemistry," *Angew. Chem. Int. Ed. Engl.* **58**(2), 442–446 (2019).
32. Y. Wang, S. Schlucker, "Rational design and synthesis of SERS labels," *Analyst* **138**(8), 2224–2238 (2013).
33. B. Shan, Y. Pu, Y. Chen, M. Liao, M. Li, "Novel SERS labels: Rational design, functional integration and biomedical applications," *Coord. Chem. Rev.* **371**, 11–37 (2018).
34. B. M. DeVetter, P. Mukherjee, C. J. Murphy, R. Bhargava, "Measuring binding kinetics of aromatic thiolated molecules with nanoparticles via surface-enhanced Raman spectroscopy," *Nanoscale* **7**(19), 8766–8775 (2015).
35. D. S. Grubisha, R. J. Lipert, H.-Y. Park, J. Driskell, M. D. Porter, "Femtomolar detection of prostate-specific antigen: An immunoassay based on surface-enhanced Raman scattering and immunogold labels," *Anal. Chem.* **75**(21), 5936–5943 (2003).
36. Y. Zhou, P. Zhang, "Simultaneous SERS and surface-enhanced fluorescence from dye-embedded metal core–shell nanoparticles," *Phys. Chem. Chem. Phys.* **16**(19), 8791–8794 (2014).
37. Z. Ye, L. Lin, Z. Tan, Y.-J. Zeng, S. Ruan, J. Ye, "Sub-100 nm multi-shell bimetallic gap-enhanced Raman tags," *Appl. Surf. Sci.* **487**, 1058–1067 (2019).
38. Y. Zhou, C. Lee, J. Zhang, P. Zhang, "Engineering versatile SERS-active nanoparticles by embedding reporters between Au-core/Ag-shell through layer-by-layer deposited polyelectrolytes," *J. Mater. Chem. C* **1**(23), 3695–3699 (2013).
39. D. K. Lim, K. S. Jeon, J. H. Hwang, H. Kim, S. Kwon, Y. D. Suh, J. M. Nam, "Highly uniform and reproducible surface-enhanced Raman scattering from DNA-tailorable nanoparticles with 1-nm interior gap," *Nat. Nanotechnol.* **6**(7), 452–460 (2011).
40. Y. Ye, W. Yi, W. Liu, Y. Zhou, H. Bai, J. Li, G. Xi, "Remarkable surface-enhanced Raman scattering of highly crystalline monolayer Ti3C2 nanosheets," *Sci. China Mater.* **63**(5), 794–805 (2020).
41. J. Shen, L. Xu, C. Wang, H. Pei, R. Tai, S. Song, Q. Huang, C. Fan, G. Chen, "Dynamic and quantitative control of the DNA-mediated growth of gold plasmonic nanostructures," *Angew. Chem. Int. Ed. Engl.* **53**(32), 8338–8342 (2014).
42. B. Zhao, J. Shen, S. Chen, D. Wang, F. Li, S. Mathur, S. Song, C. Fan, "Gold nanostructures encoded by non-fluorescent small molecules in polyA-mediated nanogaps as universal SERS nanotags for recognizing various bioactive molecules," *Chem. Sci.* **5**(11), 4460–4466 (2014).
43. N. G. Khlebtsov, L. Lin, B. N. Khlebtsov, J. Ye, "Gap-enhanced Raman tags: fabrication, optical properties, and theranostic applications," *Theranostics* **10**(5), 2067–2094 (2020).